


2016

Development of durable superhydrophobic materials for ice- and snow-free airport concrete pavements

Therin Jamal Young
Iowa State University

Follow this and additional works at: <http://lib.dr.iastate.edu/etd>

 Part of the [Civil Engineering Commons](#), and the [Mechanical Engineering Commons](#)

Recommended Citation

Young, Therin Jamal, "Development of durable superhydrophobic materials for ice- and snow-free airport concrete pavements" (2016). *Graduate Theses and Dissertations*. 15851.
<http://lib.dr.iastate.edu/etd/15851>

This Thesis is brought to you for free and open access by the Iowa State University Capstones, Theses and Dissertations at Iowa State University Digital Repository. It has been accepted for inclusion in Graduate Theses and Dissertations by an authorized administrator of Iowa State University Digital Repository. For more information, please contact digirep@iastate.edu.

**Development of durable superhydrophobic materials for ice- and snow-free
airport concrete pavements**

by

Therin Jamal Young

A thesis submitted to the graduate faculty
in partial fulfillment of the requirements for the degree of
MASTER OF SCIENCE

Major: Mechanical Engineering

Program of Study Committee:
Sriram Sundararajan, Co-Major Professor
Halil Ceylan, Co-Major Professor
Pranav Shrotriya

Iowa State University

Ames, Iowa

2016

DEDICATION

Thanks to all the educators from Clay County Elementary/Middle School, Randolph-Clay High School, and Savannah State University who challenged me to be a high achiever. To my parents, Irene and Cleo, for instilling in me the importance of education. And to my family who have supported me endlessly throughout this journey.

TABLE OF CONTENTS

CHAPTER 1. INTRODUCTION	1
Background and Motivation	1
Research Objectives.....	4
Research Approach Summary.....	5
Thesis Organization.....	8
CHAPTER 2. LITERATURE REVIEW	10
Definitions, Classifications, and Measurement Techniques.....	10
Review of Superhydrophobic Fabrication Methods.....	13
Mechanical Durability of Superhydrophobic Coatings.....	23
CHAPTER 3. TRIBOLOGICAL BEHAVIOR AND WETTABILITY OF SUPERHYDROPHOBIC COATED ALUMINUM.....	25
Abstract	25
Introduction.....	26
Materials and Methods	29
Results and Discussion	34
Conclusions	40

CHAPTER 4. DEVELOPMENT AND PERFORMANCE EVALUATION OF SUPERHYDROPHOBIC COATED CONCRETE	42
Synopsis, Scope, and Objective	42
Research Methodology	45
Conclusions	53
CHAPTER 5. FUTURE RESEARCH AND RECOMMENDATIONS	54
Specific Findings and Limitations.....	54
Recommendations.....	55
References.....	57

CHAPTER 1. INTRODUCTION

Background and Motivation

The formation and accretion of ice on vital civil infrastructures throughout the world is a problem that engineers and scientists continue to manage. The host of problems that icing events cause include property damages, expensive repairs, numerous injuries, and the occasional loss of life due to operational failures of atmosphere-exposed surfaces. “Overhead power networks, aircraft, marine structures, wind turbines, and other exposed structures are performance compromised by ice or snow accretion and adhesion in cold regions” (Kulinich and Farzaneh, 2011). A thin layer of ice is enough to bring down power lines, burst pipes, and make roads impassable. Unexpected snowstorms in places not equipped to quickly and efficiently remove snow and ice cause complex delays and chaos for thousands of people in any given event.

Airport pavements are exposed to many weather-related events and physical loading from large aircraft that lead to early stress-related failures like cracking and buckling. For example, porous concrete can become critically saturated after snow and icing events. As the moisture within the pores freezes, the ice occupies more volume than that of the water which leads to distresses in the concrete; distresses that continue to expand with each new ice and snowing event. The inclusion of air-entraining admixtures (AEAs) in the concrete mix design helps to reduce the effects of freeze/thaw cycles by creating air voids within the concrete that provide extra space for ice expansion, thus reducing the amount of distress experienced during icing events. Du and Folliard have described the air entrainment process as a complex process that is affected by factors

such as the mixing procedure, fine and coarse aggregates characteristics, physical and chemical properties of Portland cement, and dosage and properties of the AEA (Du and Folliard, 2005). Several studies have been dedicated to the development of AEAs and the factors that affect how air voids are distributed within concrete as a result of using AEAs (Zhang, 1996, Lazniewska-Piekarczyk, 2012, Van den Heede et al., 2013).

Although AEAs help protect against distresses in concrete caused by freeze/thawing, such preventive measures for pavement preservation are only temporary and do not circumvent the fact that costly pavement reconstruction is required to regain the anti-icing effects of expired air-entrained pavement. Airports' main defense against pavement icing is the use of deicers and anti-icing techniques. De-icing strategies are used to remove snow or ice that is already bonded to a surface by use of chemicals or mechanical means or a combination of both. Anti-icing strategies are used before or in the early parts of a winter weather event for preventing the development of bonded ice or snow on a surface. Both strategies are less effective and require excessive chemicals if they are applied when surface temperatures are less than 20°F. De-icing chemical methods used to mitigate ice build-up include the use of liquids whose aqueous solutions have a much lower crystallization temperature than that of water (Boinovich and Emelyanenko, 2013). Such chemicals are ideal for the containment of icing on helicopters, airplanes, and runways. However, the necessity of repeated treatment of extended surfaces, the presence of salt that initiates corrosion, and the high costs of these chemicals make them less desirable to use for fighting ice build-up (Boinovich and Emelyanenko, 2013). Because de-icing strategies are carried out late in winter weather events, more chemicals are required than in anti-icing applications. Surfaces are also

more dangerous during the time before de-icing strategies are applied which causes inconveniences such as delays and closings for travelers, work personnel, and so on. Anti-icing strategies circumvent these challenges because they are deployed on weather exposed surfaces before or during the early stages of the snow or ice event. If anti-icing applications are planned early enough, surfaces exposed to anti-icing chemicals are not allowed to bond with ice and snow. Mechanical removal of the unbounded ice and snow from the surface is simplified thus allowing for the surfaces to be operable and safer for longer periods of time.

The repeated use of sodium and calcium chlorides on concrete ultimately leads to corrosion and mechanical failure of the cementitious materials, and deicer runoff poses environmental threats to nearby water sources and wildlife (Kaushal et al., 2005, Ramakrishna and Viraraghavan, 2005, Panno et al., 2006, Fay and Shi, 2012, Kelly, 2008). High-traffic areas such as highways and airports that experience frequent snow and icing events during the winter season must employ and compensate hundreds of workers just for snow and ice removal. Such tasks also require snow removal equipment that costs millions of dollars and maintenance that requires additional funds and workers. The effects of deicers and road salt on concrete have been studied and reported upon extensively to properly address current challenges and begin to develop innovations that circumvent their use (Hassan et al., 2002, Shi et al., 2013). Calcium magnesium acetate (CMA) is a safer alternative road deicer to replace environmentally unacceptable NaCl and CaCl₂, but its high cost weakens its chance for widespread use (Dionysiou et al., 2000, Yang et al., 1992) . Alternative technologies such as conductive concrete (Yehia and Tuan, 1999, Yehia et al., 2000, Yehia and Tuan, 2000, Yang et al., 2012), hydronic-

heated pavements and the use of phase change materials for self-heated pavements are all viable options for minimizing the use of corrosive chemicals. Self-healing concretes that contain pre-incorporated healing agents, such as CaCO_3 , retard cracks caused by corrosive deicing chemicals. Such technologies carry expensive manufacturing and construction costs that are not viable for large-scale applications and require the demolition and removal of existing concrete which incur more expenses.

Airports are then tasked with finding cost-effective, environmentally-friendly and preferably non-invasive solutions for minimizing the amount of water absorbed by paved surfaces. Traditional de-icing and anti-icing techniques provide fast and reliable solutions for controlling snow and ice build-up on paved surfaces, but the use of corrosive chemicals in anti-icing/deicing solutions pose even greater threats to exposed concrete and the environment in the long run. Even more, airports are burdened with allotting more dollars to snow removal equipment and personnel to manage and provide maintenance for anti-icing/deicing operations. Large cold region international airports, such as Minneapolis St. Paul, house and provide food to hundreds of seasonal workers who are hired and trained just for snow removal operations. Although airport managers may not foresee a total elimination of the use of SREs and deicing chemicals at airports, their use can be drastically reduced with the help of innovative technologies whose main purpose is to reduce water absorption and ice adhesion on paved surfaces.

Research Objectives

The first objective was to conduct a literature review in order to develop a strong scientific understanding of the chemistry and physics that govern the phenomena of superhydrophobicity. An extensive literature review allowed for the documentation of

candidate materials and procedures for the fabrication of superhydrophobic surfaces. Candidate materials and fabrication/coating procedures were chosen for preliminary experiments based on their viability as potential candidates for real-world applications that give heavy attention to safety, cost, and availability. The literature review was also used to help identify characterization methods for superhydrophobic surfaces so that comparisons could be made between the different coating systems and the best coating in terms of overall performance could be identified. The next objective was to deposit the chosen coating systems on substrates and measure the performance of the coatings using the identified coating characterization methods and tests. The final objective was to evaluate the experimental data and provide scientific reasoning for any observed trends among the different coating systems. The findings of this study can be used along with other existing data in this field of study to help guide future research and assist in determining the viability of using such coating systems for real-world applications.

Research Approach Summary

The *Web of Science* database was used for accessing and compiling most of the literature that was used to conduct a literature review. It is worth mentioning that the gathering of literature was a process that continued throughout the duration of this research study. As upcoming sections of the thesis will show, there are several procedures for fabricating superhydrophobic surfaces. Therefore, materials, coating procedures, and other related items were chosen with respect to their viability in experimental and real-world applications since the motivation behind this research

project stems from a real-world engineering challenge. By thinking in this way, certain materials and procedures that would have a very low chance of being accepted as efficient for industrial applications can immediately be disregarded for use in this study. Inefficiencies could include high cost, time-consuming procedures, unavailable materials, etc.

Preliminary experiments were chosen and performed by carefully replicating those published in the literature. Material cost and availability, duration and complexity of experiment, and required laboratory instruments were all documented and used for determining viable candidate coating systems for this study. After an extensive literature review and preliminary experimentation, the candidate coating system listed in Table 1 was developed. The candidate coating materials chosen were polytetrafluoroethylene (PTFE), polyetheretherketone (PEEK), zinc oxide (ZnO), and diatomaceous earth (DE). PTFE and PEEK were chosen due to their hydrophobic properties and dominant use as hydrophobic materials in the literature and industrial applications (Song et al., 2008, Ferrick et al., 2008). DE's naturally occurring micro- and nano-texture is convenient for the fabrication of superhydrophobic surfaces which require hierarchical roughness in order to achieve superhydrophobicity. DE is a low cost hydrophilic material that can be rendered hydrophobic after exposing it to a solution with low surface energy chemicals such as silanes (Polizos et al., 2014, Oliveira et al., 2013). ZnO was chosen because it is another material that has been extensively used in research to develop superhydrophobic coatings (Dai et al., 2013, Jiang et al., 2014, Li et al., 2003, Myint et al., 2013). In this study, ZnO nano-powder was part of a ZnO/PTFE composite coating system.

Table 1. Experimental coating matrix and procedures.

Coating	Solution	Sonication/Stirring time before spraying
PTFE	5 g PTFE in 75 mL acetone	10 min. sonication and 10 min. stirring
PTFE/PEEK	6 g PTFE and 2 g PEEK in 80 mL acetone	30 min. sonication
DE	6 g DE in 50 mL acetone	10 min. stirring
ZnO/PTFE	0.5 g ZnO and 1 g PTFE in 50 mL acetone	15 min. stirring
Epoxy Resin	Resin and curing agent, 2:1 ratio, respectfully. Xylene, sum of resin and curing agent volumes	Hand-stirred for 2 min.

Aluminum 6061 was chosen as the substrate material for the candidate coatings because of its availability, low cost, and easy susceptibility to surface modifications compared to harder and more expensive materials such as steel. An initial intention was to utilize aluminum substrates in the early parts of the study and later utilize Portland Cement Concrete (PCC) as the coating substrate. However, it was concluded, as will be reported in following sections, that the physical properties of concrete such as roughness and aggregate size exceeded the measurement capabilities of the available instruments necessary for this scientific study. As a result of this finding, aluminum substrates were used throughout the experimental processes.

After coatings were spray-deposited onto aluminum substrates and allowed to dry, the average roughness (R_a) and coating thickness were measured by using contact profilometry and stereomicroscope, respectfully. The wettability of the coatings was

evaluated by measuring static water contact angles on the coated surfaces. The friction coefficient, μ , was calculated by performing ramped load tests on the coated surfaces with a ball-on-flat micro tribometer. The durability of the coatings was measured by performing reciprocating wear tests via micro tribometer for a constant load. The depth of the resulting wear track was used as a quantitative measure of the coatings' resistance to wear. Scanning electron microscopy (SEM) imaging was used to view the topographical structure of the candidate coatings, and energy dispersive spectroscopy (EDS) was used to analyze the chemical nature of the coatings after being exposed to wear.

The tools and experimental instruments used for performing tests and analysis of the coating systems were chosen based on their proven success in current literature relevant to this field of study and their availability at Iowa State University. Any instruments or materials deemed necessary for this study that were not available at Iowa State University were purchased.

Thesis Organization

The thesis is organized into five chapters. Chapter 1 has provided an introduction to the research problem. Chapter 2 consists of a literature review which provides definitions, measurement techniques, and classification systems for hydrophobicity, superhydrophobicity, and icephobicity. The methods for fabricating superhydrophobic surfaces will also be reported and listed in Chapter 2. Chapter 3 will focus entirely on the laboratory experiments that were used to evaluate the tribological behavior and

wettability of the previously mentioned four candidate coatings on aluminum, and Chapter 4 will report the findings associated with superhydrophobic coatings on concrete. It should be noted that the efforts of Chapter 3 reflect the research objectives more than the efforts of Chapter 4 since the used experimental instruments were effective on aluminum and not concrete. The thesis will be concluded with Chapter 5 in which conclusions, recommendations, and limitations of the study will be reported. Chapter 5 will also include recommendations for further research and the potential contribution of this study to current and future engineering practices.

CHAPTER 2. LITERATURE REVIEW

Definitions, Classifications, and Measurement Techniques

A surface is said to be hydrophobic if it repels water and hydrophilic if it adsorbs or is wetted by water. The strength of the cohesive forces present within the water molecule and the cohesive forces associated with the interaction of the water and the surface determine the wettability of that surface. If the cohesive forces within the water molecule are greater than those of the surface it rests on, water drops will bead up and not wet the surface.

The surface energies on the surface of a coating are usually either homogenous or heterogeneous, and these two states are characterized by the Wenzel (Wenzel, 1936) and Cassie-Baxter (Cassie and Baxter, 1944) models, respectively. Wenzel proposed that surface roughness is directly proportional to the wettability of a surface. A hydrophobic surface that is roughened will become more hydrophobic, and a roughened hydrophilic surface will become more hydrophilic. The Wenzel model describes an event where the liquid droplet enters the grooves therefore resulting in a lower contact angle because of the increase in contact area. R is the ratio of the actual area of the solid/liquid interface to the normally projected area. In the Cassie-Baxter model, air is trapped in between the roughness asperities thus creating an event in which the liquid-solid contact area is decreased and water contact angle is increased. The term f is the fraction of the solid/liquid interface in the entire composite surface beneath the liquid. Cassie's model is an extension of Wenzel's in that it assumes a rough surface with pores.

$$\text{Wenzel Model: } \cos\theta_w = R\cos\theta$$

$$\text{Cassie - Baxter Model: } \cos\theta_{C-B} = f - 1 + f\cos\theta$$

The wettability of a surface is reliable on the critical surface tension of that surface. If a liquid has a surface tension that is lower than the surface's critical surface tension, then that liquid will wet the surface and exhibit a low contact angle. Thus, surfaces can be chemically treated to reduce the critical surface energy and increase the water contact angle. Superhydrophobic surfaces are identified as having static contact angles greater than 150 °. It is important to note that the gravitational force and size of the water droplet affect the measured water contact angle on a super hydrophobic surface. For water contact angle measurements that require the use of image analysis tools, the fitting mode used to measure the contact angle of the droplet is also important. Fitting modes include elliptic fitting, circle fitting, tangent searching, Laplace-Young fitting and so on. Tangent searching was utilized for the studies of this thesis. Experimental data shows the water contact angle to be no more than 156 degrees for a 4 or 5 μL water droplet using elliptic fitting (Zhang et al., 2008a). The low surface energy of superhydrophobic surfaces cause water drops of higher surface energies to make minimal contact with the surface; thus creating spherical droplets that do not wet the surface. Such surfaces exist in nature on the lotus leaf and on the legs of the water strider. In regards to the lotus leaf, the wax of the leaf is hydrophobic but not enough to explain the superhydrophobic effect

(Herminghaus, 2000). It has been proven that the characteristic roughness of the leaves is what causes the superhydrophobic effect. This implies that a surface is rendered superhydrophobic by imposing additional roughness on a hydrophobic surface and decreasing the liquid/solid contact area.

As mentioned, superhydrophobic coatings have potential applications on surfaces in cold regions that experience extreme icing events. Therefore, a review of literature that addresses icephobicity was necessary for this study. The term “icephobic” has been under debate for some time (Hejazi et al., 2013). Icephobic surfaces are believed to delay the formation of the ice nucleus and reduce adhesive forces between ice and surface (Hejazi et al., 2013, Meuler et al., 2010, Zheng et al., 2011, Jung et al., 2011, Menini and Farzaneh, 2009, Jung et al., 2012, Guo et al., 2012). Studies have shown that hydrophobic (Saito et al., 1997, Somlo and Gupta, 2001) and superhydrophobic coatings (Guo et al., 2012, Cao et al., 2009) can possess ice-repellent properties. Early studies of icephobic surfaces have focused on droplet-on-liquid interactions because they ultimately affect ice build-up. Braziers.Pr et al found that the coalescence of the two liquid volumes can be prevented permitted that conditions allow for a film of gas to be trapped between the respective volumes of liquid (Braziers.Pr et al., 1972). This concept of using thin films of entrapped air to prevent two surfaces from bonding is similar to earlier theories of superhydrophobicity reported by Cassie and Baxter (Cassie and Baxter, 1944). Therefore, it is plausible to apply concepts and ideas of superhydrophobicity when studying icephobicity.

Review of Superhydrophobic Fabrication Methods

Several physical and chemical modifications have been used to create desired roughness on substrate surfaces to vary the surface wettability. These methods include wax solidification, lithography, vapor deposition, template method, polymer reformation, sublimation, electrospinning, plasma techniques, sol gel processing, electrochemical methods, bottom-up approach for the fabrication of nano-arrays, and hydrothermal synthesis.

Superhydrophobic surfaces are created by a combination of hierarchical surface roughness and low surface energy materials. Hydroxyl groups on surfaces are a key site for hydrogen bonding and the reason why surfaces are wettable. When the hydroxyl sites are masked by hydrophobic silane surface treatments, the surface energy is reduced and the surface is rendered hydrophobic or superhydrophobic depending on other topographical features.

Boinovich et al have reported three criteria associated with attaining a surface that has superhydrophobic properties. First hydrophobic agents must be applied to the material in order to decrease the material's surface energy if the surface is not naturally hydrophobic. Second, an appropriate shape of textural elements is chosen for increasing the local contact angle of the textured surface. And third, a surface with multimodal roughness properties must be created (Boinovich and Emelyanenko, 2013). Table 2 lists a summary of the fabrication methods discussed in the following sections.

Wax Solidification

Past studies show that rough fractal surfaces form as a result of the solidification of melted waxes such as alkylketene dimer (AKD). AKD exhibits natural hydrophobic properties as a result of the presence of alkyl molecules that are immiscible in water. Shibuichi et al controlled the water-repellency and roughness of ADK and dialkylketone (DAK) coatings on glass substrates by controlling the ratio of AKD and DAK mixed. It was shown that roughness increased as the amount of DAK was increased in the mixture resulting in water contact angles greater than 170 degrees after 3 days of solidification in a dry N₂ gas atmosphere at room temperature(Shibuichi et al., 1996). Fang et al reported similar relationships between fractal growth and solidification time when using triglycerides as the wax coating. In Fang's study, the rate of the wax's transition from a metastable to stable crystalline and the wettability of the fractal surface was dependent on the melting temperature and the molecular size (Fang et al., 2007).

Sol Gel Processing

The mechanical robustness and low cost of sol gels make them a desirable candidate for fabricating non-wetting surfaces. Sol gel processing can be used to fabricate coatings that are antireflective and durable for use as antireflective coatings for optics that experience extreme working conditions (Pilipavicius et al., 2008, San Vicente et al., 2009). Manca et al produced a superhydrophobic coating that was composed of sol-gel-processed organosilica binder embedded with silanized nanospheres (Manca et al., 2009). Dai et al used a PDMS mold to replicate the microstructures of a fresh lotus leaf and then imprinted the microstructure onto a sol film via sol gel processing (Dai et

al., 2013). A low-temperature hydrothermal process then allowed the growth of nano-ZnO structures which introduced a hierarchical roughness on the surface.

Lithography

Lithography is an inexpensive technique that allows for the fast fabrication of large-scaled micro- and nano-structured surfaces. Lithography is usually used in combination with other fabrication processes like chemical and plasma etching to further change physical and chemical properties of the surface for applications such as anti-wetting and self-cleaning. Nanosphere lithography and oxygen plasma etching have been used to disperse large-area periodic nanosphere arrays by controlling the spin speed and amount of surfactant in the nano particle solution (Shiu et al., 2004). A similar nano-imprint lithography procedure has been used along with wet chemical etching (Pozzato et al., 2006). Suh et al used capillary lithography to fabricate nano-pillars on polyethylene glycol surfaces by using negative and positive polymeric molds (Suh and Jon, 2005). It was shown that as the height of the nano-pillars increased so did the static water contact angle as a result of more air entrapment between the pillars.

Vapor Deposition

Chemical vapor deposition (CVD) is a widely used method for depositing thin films on substrates. Wu et al deposited durable and optically transparent thin films via microwave enhanced plasma CVD. By varying between partial and total pressure during the vapor deposition process, the durability and wettability of the coatings were studied. It was noted that the partial pressure had more influence on the mechanical durability of the coatings while the total pressure had more influence on the chemical characteristics (Wu et al., 2004). Saini et al have also developed hydrophobic and superhydrophobic

coatings via CVD by using an adhesion promoter within the deposition process that results in a more robust coating (Saini et al., 2008). Crick and Parkin used aerosol-assisted CVD to fabricate copper films on substrates that could be compositionally-controlled by varying substrate temperature and the solvent used. After functionalization of the coatings with a low surface energy silane, water contact angles nearly reached 180 degrees (Crick and Parkin, 2011).

Template Method

Feng et al demonstrated that by confining amphiphilic PVA to nano-sized spaces of a template, the hydrophobic molecules of the PVA solution could be rearranged and moved to the outer rough surface of the resulting PVA fiber which results in lower surface free energy and anti-wetting properties of the coating (Feng et al., 2003). Jin et al fabricated tightly-packed polystyrene nanotubes on glass substrates by using a porous template of commercial aluminum membranes. The van der Waals forces present between the closely-packed nanotubes were believed to increase the adhesion force between the nanotubes and water droplets (Jin et al., 2005). Therefore, the surface was superhydrophobic, but the water drops were not allowed to slide as a result of the high adhesion forces. Chen et al used a carbon template method in which hollow spheres were fabricated on a glass substrate as a result of a calcination process (Chen et al., 2012). An additional CVD process was used to increase the stability of the coating.

Electrochemical Methods

Li et al developed a conductive hydrophobic ZnO thin layer via electrochemical deposition. Further functionalization of the surface with a low surface energy silane led to superhydrophobic ZnO coatings. It was seen that when electrochemical depositions were

carried out at cathodic voltages in the range of -2 to 3 V for extended amounts of time, the morphology of the thin films could be controlled to consist of rough nanocrystals which further reduce surface energy (Li et al., 2003). Shi et al used a combination of layer-by-layer coating and electrochemical deposition in order to fabricate gold threads with micro- and nano-sized gold particles. Further functionalization of the gold threads with a low surface energy material caused the threads to be able to float on water and mimic the legs of a water strider (Shi et al., 2006). Shi et al also developed a facile method for fabricating a silicon substrate with gold nanoparticles by using a galvanic cell reaction. The process involved dipping the Si wafer into a solution of the metal ion and HF which required no additional instruments (Shi et al., 2005).

Bottom-Up Approach for the Fabrication of Nano-Arrays

Traditional top-down approaches for fabrication of superhydrophobic surfaces leave little room for controlling the morphology of surfaces with nanometer resolution due to high surface area fractions of the used materials. Hosono et al used a bottom-up process to fabricate needle-like structures with low surface area fractions based on metal hydroxides. The bottom-up process allowed for controlling the morphology of the needles on the order of several nanometers because the tip of the needles contained very few atoms (Hosono et al., 2005). Thermodynamic equilibrium conditions of a chemical bath deposition process allowed for each needle to be deposited individually. Srinivasan et al have used the bottom-up approach for the self-assembly of nano-composites consisting of multi-walled carbon nanotubes and oligo (p-phenylenevinylene)s with self-cleaning properties (Srinivasan et al., 2008). Hatton and Aizenberg used the bottom-up approach

in developing a method to engineer selectively functionalized nanowire post tips that could be used to control particle attachment (Hatton and Aizenberg, 2012).

Hydrothermal Synthesis

Wang et al used an in situ hydrothermal process to fabricate a titanium substrate with nanolamellate structures of CaTiO_3 . The density of nanolamellate structures could be tuned by varying the reaction times and NaOH concentrations (Wang et al., 2007). The nanolamellate structures were completely converted from superhydrophilic to superhydrophobic after spin-coating a layer of hydrophobic silicone onto the surface. Similar processes have been used to fabricate superhydrophobic CuO (Basu et al., 2011) and ZnO (Si and Xue, 2009) surfaces.

Table 2 Summary of superhydrophobic fabrication methods

Title of Publication	Author(s)	Materials and Processing	Year
Hydrophobic Antireflective Silica Coatings via Sol-gel Process	Pilipavicius et al.	Colloidal SiO_2 nanoparticles, sol-processing, hexamethyldisilazane (HMDS) methyltrimethoxysilane (MTMS)	2008
Durable Superhydrophobic and Antireflective Surfaces by Trimethylsilanized Silica Nanoparticles-Based Sol-Gel Processing	Manca et al.	Sol-gel processing, organosilica binder, trimethylsilanized nanospheres, double-layer	2009

Table 2 continued

Long-term durability of sol-gel porous coatings for solar glass covers	San Vicente et al.	Sol-gel silica porous coatings, solar transmittance, durability	2009
Biomimetic fabrication and tunable wetting properties of three-dimensional hierarchical ZnO structures by combining soft lithography template with lotus leaf and hydrothermal treatments	Dai et al.	Fresh lotus leaf, ZnO sol film, soft lithography, hydrothermal reaction	2013
Spontaneous Formation of Fractal Structures on Triglyceride Surfaces with Reference to Their Super Water-Repellent Properties	Fang et al.	Wax solidification of Alkylketene dimer (AKD) for superhydrophobicity	2006
Formation mechanism of super water-repellent fractal surfaces of alkylketene dimer	Fang et al.	Wax melt-solidification of alkylketene dimer (AKD) for superhydrophobicity	2008

Table 2 continued

Super Water-Repellent Surfaces Resulting from Fractal Structure	Onda et al.	Wax melt-solidification of AKD for superhydrophobicity	1996
Superhydrophobic surfaces fabricated by nanoimprint lithography	Pozzato et al.	Nanoimprint lithography and wet chemical etching on silicon for superhydrophobic surfaces	2006
Fabrication of Tunable Superhydrophobic Surfaces by Nanosphere Lithography	Shiu et al.	Nanosphere lithography and oxygen plasma treatment for tunable superhydrophobicity	2004
Control over Wettability of Polyethylene Glycol Surfaces Using Capillary Lithography	Suh and Jon	Capillary lithography for tuning wettability of polyethylene glycol surfaces	2005
CVD of copper and copper oxide thin films via the in situ reduction of copper (II) nitrate –a route to conformal superhydrophobic coatings	Crick and Parkin	Aerosol-assisted chemical vapour deposition of copper (II) nitrate for superhydrophobic coating	2011
Two-silane chemical vapor deposition treatment of polymer (nylon) and oxide surfaces that yields hydrophobic (and superhydrophobic), abrasion-resistant thin films	Saini et al.	Chemical vapor deposition using adhesion promoter for abrasion-resistant superhydrophobic coatings	2008

Table 2 continued

Mechanical durability of ultra-water-repellent thin film by microwave plasma-enhanced CVD	Wu et al.	Chemical vapor deposition using partial pressure to enhance durability of superhydrophobic coatings	2004
Creation of a Superhydrophobic Surface from an Amphiphilic Polymer	Feng et al.	Templating method for fabricating PVA nanofiber	2003
Superhydrophobic Aligned Polystyrene Nanotube Films with High Adhesive Force	Jin et al.	Templating polystyrene nanotube films for superhydrophobicity	2005
Controlled growth of carbon spheres by chemical vapor deposition based on anodic aluminum oxide nano-template	Chen et al.	Aluminum oxide nano-template for controlled growth of carbon spheres	2012
Electrochemical Deposition of Conductive Superhydrophobic Zinc Oxide Thin Films	Li et al.	Electrochemical deposition of conductive hydrophobic zinc oxide for superhydrophobicity	2003
Facile Method To Fabricate a Large-Scale Superhydrophobic Surface by Galvanic Cell Reaction	Shi et al.	Galvanic cell reaction for chemical-deposition of Ag nanostructures	2006

Table 2 continued

Combining a Layer-by-Layer Assembling Technique with Electrochemical Deposition of Gold Aggregates to Mimic the Legs of Water Striders	Shi et al.	Layer-by-Layer and electrochemical deposition of Ag aggregates for superhydrophobicity	2005
Superhydrophobic Perpendicular Nanopin Film by the Bottom-Up Process	Hosono et al.	Bottom-up process of metal hydroxides for superhydrophobicity	2005
Bioinspired Superhydrophobic Coatings of Carbon Nanotubes and Liner pi Systems Based on the "Bottom0up" Self-Assembly Approach	Srinivasan et al.	Bottom-up approach for self-assembly of multi-walled carbon nanotubes with self-cleaning properties	2008
Writing on Superhydrophobic Nanopost Arrays: Topographic Design for Bottom-up Assembly	Hatton et al.	Bottom-up process for functionalized nanowire post tips	2012
In situ hydrothermal synthesis of nanolamellate CaTiO ₃ with controllable structures and wettability	Wang et al.	Hydrothermal synthesis of CaTiO ₃ for controllable wettability	2007

Table 2 continued

Fabrication and Functionalization of CuO for Tuning Superhydrophobic Thin Film and Cotton Wool	Basu et al.	Thin Film CuO by hydrothermal synthesis for superhydrophobicity	2011
Hydrothermal Fabrication of Core-Shell Structured Cu ₂ O Microspheres via an Intermediate-Template Route	Si and Xue	Hydrothermal fabrication Cu ₂ O microspheres using template route	2009

Mechanical Durability of Superhydrophobic Coatings

Coating durability can depend on several factors including substrate and film properties, micro/nano structure of coating materials, and strength of the coating matrix. Gemici et al reported that the extreme thinness (100 nm) and high porosity of hydrothermally-fabricated nanoparticle-containing films most likely increased the scratch resistance of the films compared to nanoparticle films that were fabricated with a high-temperature calcination process (Gemici et al., 2008). Jung et al assessed the mechanical durability of a composite superhydrophobic carbon nanotube coating by using an epoxy as the matrix for the coating. Reports showed that the coatings maintained substrate adherence and superhydrophobicity after performing cyclic wear tests at pressures ranging from 100 nN via AFM to 10 mN via ball-on-flat tribometer (Jung and Bhushan, 2009). Xiu et al showed that coatings composed of hierarchically structured micro/nano roughness can retain superhydrophobic properties even after

prolonged exposure to mechanical wear and extreme environmental conditions because only the tops of microstructures are damaged during abrasion (Xiu et al., 2012). The surface areas that are not directly exposed to abrasion retain their hierarchical roughness and thus retain hydrophobicity but with higher contact angle hysteresis.

CHAPTER 3. TRIBOLOGICAL BEHAVIOR AND WETTABILITY OF SUPERHYDROPHOBIC COATED ALUMINUM

Modified from a paper to be submitted to *Wear of Materials*

T. Young¹, J. Jackson¹, S. Roy¹, H. Ceylan², S. Sundararajan¹

¹*Mechanical Engineering, Iowa State University, Ames, Iowa 50010*

²*Civil, Construction, and Environmental Engineering, Iowa State University, Ames, Iowa 50010*

Abstract

Superhydrophobic surfaces that mimic surfaces found in nature, such as the lotus leaf, are an attractive research topic in various fields of study because of their numerous applications. More recent studies have focused on superhydrophobic surfaces that reduce or completely stop the accretion of ice and snow on power lines and aircraft that operate in cold regions. The superhydrophobic phenomena is usually achieved by creating a dual-scale roughness that is composed of micro- and nano-scale structures that trap air in-between themselves and reduce the surface energy of the textured surface. The objective of this study was to assess the tribological behavior of micro/nano particle based superhydrophobic coating mixtures composed of PTFE, composite PTFE/PEEK, diatomaceous earth (DE), and composite PTFE/ZnO that can be potential candidates for anti-wetting and anti-icing applications for transportation systems.

*Corresponding author: srirams@iastate.edu

A contact profilometer was used to measure and characterize the average roughness and thickness of coatings.

Coating wettability was assessed by measuring the tangent-line contact angle of static water drops on coated surfaces. Friction and cyclic abrasive wear tests were conducted via ball-on-flat tribometer using a spherical tungsten probe at room temperature. Scanning electron microscopy was used to characterize the physical and chemical properties of the coatings and identify the wear mechanisms. The results showed that all coatings except ZnO/PTFE exhibited superhydrophobicity. Abrasive wear mechanisms were the dominant modes for the coatings. PTFE and ZnO/PTFE coatings displayed good wear resistance, superior to that of the DE and PTFE/PEEK coatings.

Introduction

The formation and accretion of ice on vital infrastructure throughout the world is a challenge that engineers and scientists work to control. The host of problems that icing events cause include property damages, expensive repairs, numerous injuries, and the occasional loss of life due to operational failures of atmosphere-exposed surfaces. A thin layer of ice is enough to bring down power lines, burst pipes, and make roads impassable. The common approaches for reducing ice adhesion on vital infrastructures include mechanical (Makkonen, 2013), electro thermal (Boinovich and Emelyanenko, 2013), and conventional methods such as the use of de-icing salts and anti-freezing aqueous solutions on highways.

An alternative approach is to utilize the water-repellent properties of superhydrophobic coatings to minimize the pooling of water. A superhydrophobic surface is characterized as having a water contact angle greater than 150° and a sliding contact angle of less than 15° . Such surfaces have been studied extensively over the last decade and consist of a variety of fabrication methods, materials, and applications (Pilipavicius et al., 2008, San Vicente et al., 2009, Manca et al., 2009, Dai et al., 2013). Only recently have superhydrophobic coatings been considered as alternatives for reducing ice adhesion on transportation infrastructure (Flores-Vivian et al., 2013, Horgnies and Chen, 2014). There is a need to study the tribological behavior and mechanical durability of superhydrophobic coatings in order to effectively evaluate their feasibility for real-world transportation infrastructure applications.

Coating durability can depend on several factors including substrate and film properties, micro/nano structure of coating materials, and strength of the coating matrix. Gemici et al reported that the extreme thinness (100 nm) and high porosity of hydrothermally-fabricated nanoparticle-containing films most likely increased the scratch resistance of the films compared to nanoparticle films that were fabricated with a high-temperature calcination process (Gemici et al., 2008). Jung et al assessed the mechanical durability of a composite superhydrophobic carbon nanotube coating by using an epoxy as the matrix for the coating. Reports showed that the coatings maintained substrate adherence and superhydrophobicity after performing cyclic wear tests at pressures ranging from 100 nN via atomic force microscopy to 10 mN via ball-on-flat tribometer (Jung and Bhushan, 2009). Xiu et al showed that coatings composed of hierarchically structured micro/nano roughness can retain superhydrophobic

properties even after prolonged exposure to mechanical wear and extreme environmental conditions because only the tops of microstructures are damaged during abrasion (Xiu et al., 2012). The surface areas that are not directly exposed to abrasion retain their hierarchical roughness and thus retain hydrophobicity but with higher contact angle hysteresis.

In this study, four candidate hydrophobic materials were spray deposited onto aluminum substrates. A commercial polymer binder was incorporated into the coating procedure to promote substrate/coating adhesion and coating durability. The wear resistance of the coatings was assessed by performing ball-on-flat abrasion tests via micro tribometer and measuring the average depth of the resulting wear tracks with a contact profilometer. Friction coefficients were measured and analyzed among different coating combinations to monitor the change in friction before and after coatings were deposited. Scanning electron microscopy (SEM) and energy dispersive spectroscopy (EDS) provided additional analysis of the tribological behavior of coatings as a result of wear testing.

Materials and Methods

Substrate Preparation

Aluminum 6061 was used as the substrate material. The thickness of the aluminum plates were was 0.32 cm as listed by Fisher Scientific. A Buehler Ecomet III variable speed polisher with an 8-inch grinding wheel was used to roughen the surface of 5 cm x 5 cm aluminum plates. Polishing was performed by first abrading the aluminum surface with a coarse 60-grit abrasive disk for 60 seconds followed by a less-coarse 240-grit abrasive disk for 60 seconds. The resulting R_a of the abraded surfaces was measured in five locations with a contact profilometer over a scan length of 3 mm, and the average and standard deviation were recorded. Surface roughness after polishing resulted in fairly uniform surfaces with comparable R_a values of the resulting samples. The polished aluminum substrates were subsequently cleaned by sonication in an acetone bath for 10 minutes and in an ethanol bath for 10 minutes. Cleaned substrates were dried at room temperature and stored in a desiccator cabinet until coating deposition.

Coating Preparation

The micro/nano particle-based coating systems selected for this study were polytetrafluoroethylene (PTFE), polytetrafluoroethylene/polyetheretherketone (PTFE/PEEK), zinc oxide/polytetrafluoroethylene (ZnO/PTFE), and diatomaceous earth (DE). These materials were selected for their successful use as superhydrophobic materials in previous studies (Song et al., 2008, Polizos et al., 2014, Oliveira et al., 2013, Dai et al., 2013). Each material was prepared as described in this section and spray-coated onto the aluminum substrate using the layer-by-layer process shown in

Figure 1. Table 3 provides an overview of the preparation of the coating/solvent materials prior to deposition.

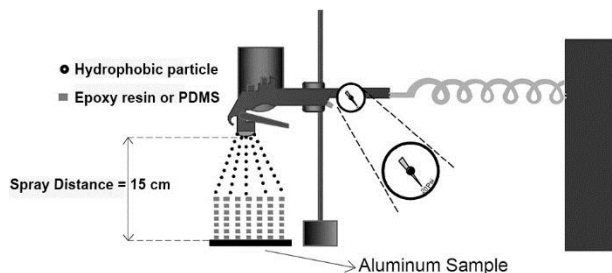


Figure 1. Schematic of spray-coating setup.

EPON Resin 1002F epoxy resin was purchased from Ellsworth Adhesives (www.ellsworth.com). Acetone and xylene were used as solvents in coating preparation. An epoxy solution was sprayed onto the aluminum substrate prior to spraying on the hydrophobic material coatings. The epoxy resin mixture was prepared 5 minutes prior to the completion of each of the respective coatings so as to reduce the sitting time of the epoxy resin. The two-part epoxy consisted of the epoxy resin and a curing agent. Xylene was used to further decrease the viscosity of the epoxy/curing agent mixture. The volume ratio used for the epoxy and curing agent was 2:1 and the volume of xylene used was the sum of the volumes of the epoxy and the curing agent. The epoxy solution was stirred for 120 seconds and immediately added to the spray gun feed.

Table 3. Overview of coating preparation prior to deposition

Coating	Solution	Sonication/Stirring time before spraying
PTFE	5 g PTFE in 75 mL acetone	10 min. sonication and 10 min. stirring
PTFE/PEEK	6 g PTFE and 2 g PEEK in 80 mL acetone	30 min. sonication
DE	6 g DE in 50 mL acetone	10 min. stirring
ZnO/PTFE	0.5 g ZnO and 1 g PTFE in 30 mL acetone	15 min. stirring
Epoxy Resin	Resin and curing agent, 2:1 ratio, respectfully. Xylene, sum of resin and curing agent volumes	Hand-stirred for 2 min.

Zonyl MP1300 PTFE powder with an average particle diameter of 12 μm was donated by DuPont. A PTFE/acetone mixture consisting of 5 g PTFE powder and 75 mL acetone was sonicated for 10 minutes to disperse the PTFE particles in acetone. PTFE particle dispersion in acetone was poor after sonication due to the low surface energy of the PTFE particles. Additional stirring of the mixture at 600 rpm for 10 minutes yielded improved PTFE particle dispersion for a longer amount of time. PTFE/acetone mixtures were spray-deposited within 10 seconds of being emptied into the spray gun feed as to avoid depositing coatings with poor particle dispersion.

Vestakeep PEEK powder with average particle diameter of 50-80 μm was purchased from Evoniks. PEEK and PTFE powders were mixed in 80 mL acetone with a 3:1 ratio, respectively. The composite mixture was sonicated for 30 minutes before being spray deposited.

ZnO (99+%) nanopowder with an average particle diameter of 10-30 nm was purchased from US-Nano. A ZnO/PTFE composite mixture consisting 0.5g ZnO powder and 1 g PTFE powder was stirred at 600 rpm in 100 mL acetone for 15 minutes.

Diatomaceous earth powder composed of naturally occurring micro- and nano-textured diatoms was purchased from Fisher Scientific. 1H, 2H, 2H-perfluorodecyltriethoxysilane (PFDTs) was purchased from Sigma Aldrich. The DE coating solution was prepared following the procedures outlined in a previous study (Polizos et al., 2014). A 10:1 weight ratio of DE and PFDTs was dispersed in hexane and magnetically stirred for 24 hours at 600 rpm. Upon stirring, the hexane completely evaporated and the remaining silanized DE powder was rinsed over filter paper with hexane to get rid of any residuals or non-bonded silane groups (Oliveira et al., 2013, Polizos et al., 2014). Afterwards, the silanized DE powder was dried in an oven at 150°F for two hours. For the coating procedure, 6 g of silanized DE was added to 50 mL of acetone and stirred at 600 rpm with a magnetic stirrer for 10 minutes.

Substrate and Coating Characterization

Coating thickness was measured with a Nikon SMZ 745T stereo microscope. Coated aluminum samples were positioned upright in a custom holder to ensure focusing of the coating/substrate cross-section. A calibrated image analyzer tool was then used to measure the coating thickness in the captured image. A Dektak IIA contact profilometer was used to measure the roughness (R_a) of the aluminum substrate and

coatings. The scan length of each measurement was 3 mm and the horizontal resolution was 25 microns per data point for an estimated 80-200 data points.

Coating wettability was quantified by measuring the static water contact angle of the coated surface. A 4 μL water droplet was deposited on the sample surface, and an image of the droplet/substrate interaction was captured with a high magnification digital camera. The average static water contact angle was measured with an on-screen protractor by using the sessile-drop and tangent line method. A contact angle measurement was taken on both sides of the water droplet and the two angles were averaged. Ten water droplets were measured on each sample for a total of twenty contact angle measurements. All measurements are reported as an average along with a 90% confidence interval.

Friction and Wear Tests

Friction and wear tests were performed on candidate coatings via ball-on-flat micro tribometer under dry sliding conditions. A schematic of the instrument used is shown in Figure 2. The coefficient of friction on the coatings was measured by performing ramped load tests. For the ramp load tests, the probe was scanned across the coated surface for a distance of 10 mm while the load was ramped from 0 to 40 mN at a speed of 3 mm/s. Reciprocating wear tests were performed on the coatings using a normal load of 40 mN for 10 and 25 cycles. The depth of resulting wear tracks was then measured at five locations with the Dektak IIA contact profilometer to quantify the wear resistance of the coatings. A FEI Quanta 250 field-emission SEM was used to image

and analyze the structural information of the coated surfaces and also help to determine the mode of wear for the reciprocating wear tests. The SEM was operated at a voltage of 10 kV and under low vacuum conditions to capture images of 10- and 25-cycle wear track areas. The secondary and backscatter electron detectors were used for imaging wear tracks depending on the shallowness of the wear track. The EDS system was used to detect potential changes in the composition of elements inside and outside of the wear track area.

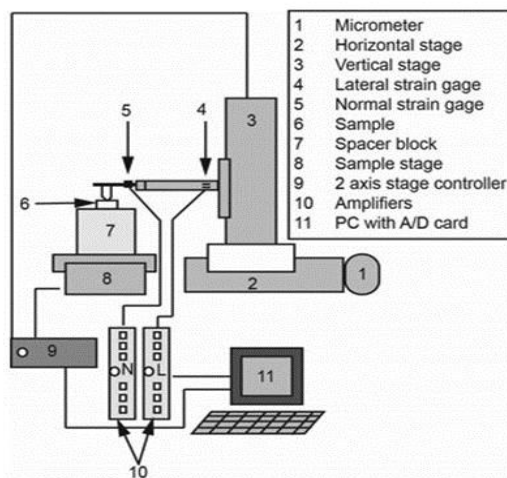


Figure 2. Schematic of ball-on-flat reciprocating tribometer.

Results and Discussion

Coating Characterization

Figure 3 shows the comparative coating thicknesses and R_a of the coatings. The average thickness of PTFE, PTFE/PEEK, ZnO/PTFE, and DE coatings was 138 ± 4.7

μm , $170 \pm 11.5 \mu\text{m}$, $148 \pm 8.9 \mu\text{m}$, and $138 \pm 6.4 \mu\text{m}$, respectively. The R_a of coated surfaces shown in Figure 4 was assessed to help explain the topographical features that may influence surface wetting states such as the Cassie-Baxter (Cassie and Baxter, 1944) and Wenzel (Wenzel, 1936) and to study any correlation between surface roughness and resulting behavior of the coatings. PTFE/PEEK and DE/EP coatings displayed R_a values that were slightly higher than the other sample coatings. The SEM images in Figure 5 shows the structure of the four coatings.

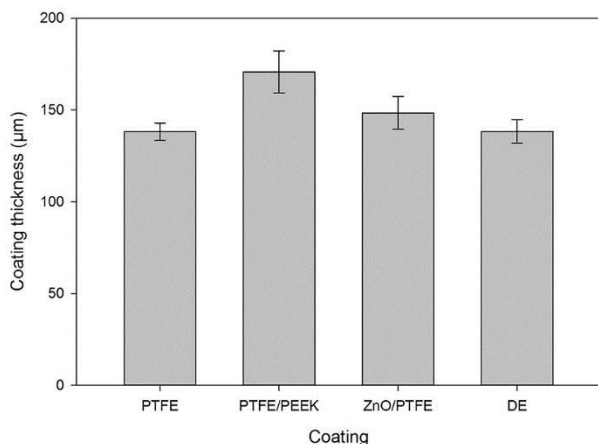


Figure 3. Coating thickness.

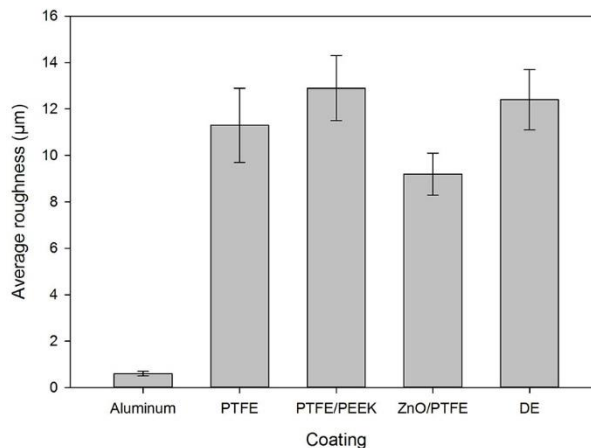


Figure 4. Average coating roughness.

The higher R_a values for PTFE, PTFE/PEEK and DE coatings are attributed to the hierarchical structure these coatings exhibit compared to ZnO/PTFE as inferred from the SEM images. Although PTFE is relatively monodisperse compared to PTFE/PEEK and DE, Figure 5 suggests a structure influenced by agglomeration or aggregation during the deposition process. This contributes to a structure that exhibits some level of hierarchy. For the PTFE/PEEK composite coating, the observed hierarchical structure is facilitated by the differences in sizes between PTFE (12 μm diameter) and PEEK (50-80 μm diameter). The ZnO/PTFE coating exhibits a more uniform surface as compared to the other coatings despite the presence of the smaller ZnO particles and larger PTFE

particles. While the average particle size of the DE powder was not measured for this study, the reported natural micro/nano texture of DE particles (Oliveira et al., 2013, Polizos et al., 2014) is believed to result in a hierarchical structure. The nano-textured surface can be seen on the cylindrical DE particles in Figure 5.

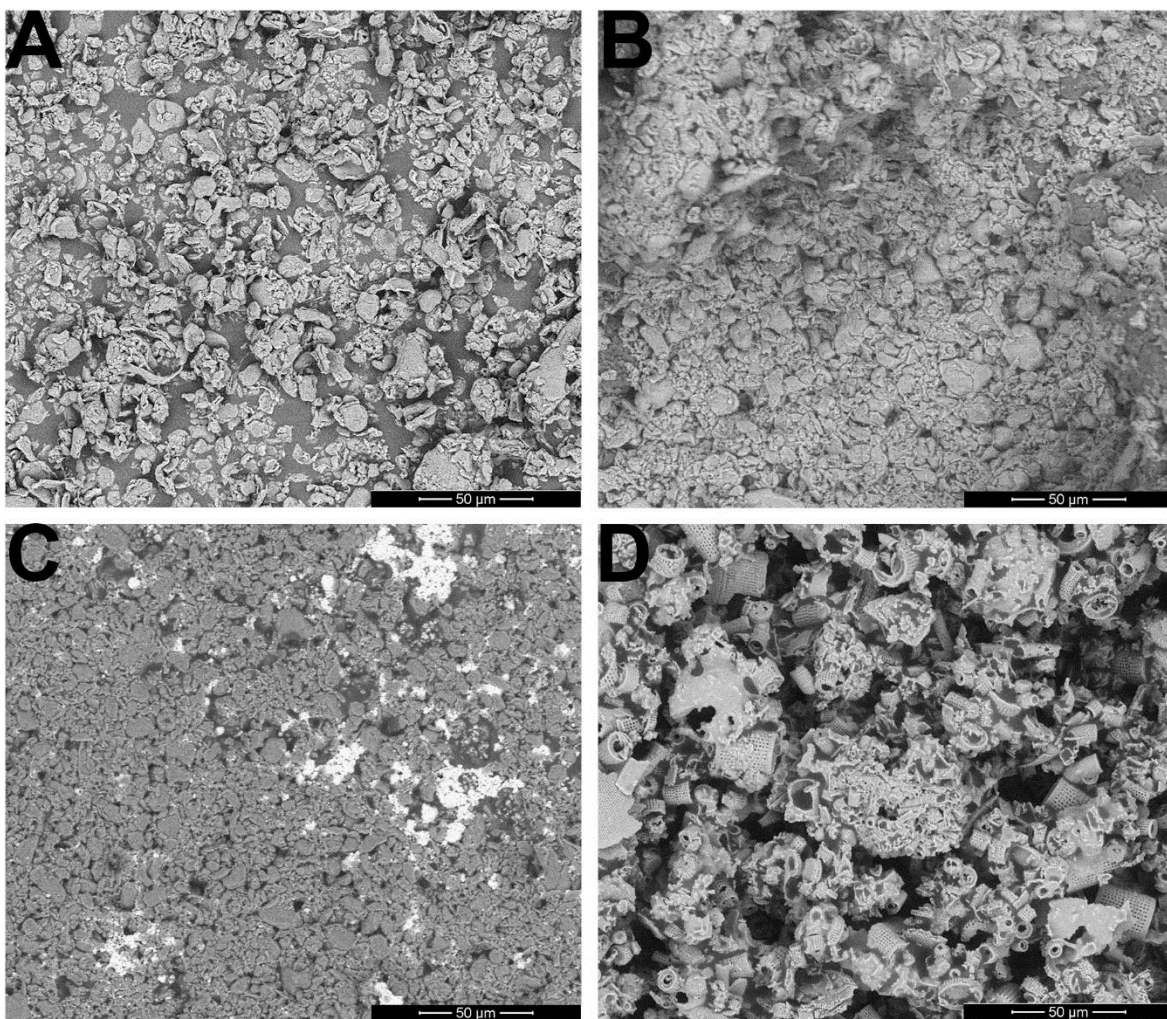


Figure 5. SEM micrographs of coatings A) PTFE B) PTFE/PEEK C) ZnO/PTFE D) DE.

Figure 6 shows the results of the water contact angle measurements on the coatings. All the coatings except ZnO/PTFE exhibited static water contact angles above 150° which is characteristic of superhydrophobicity. This behavior of PTFE, PTFE/PEEK and

DE is consistent with the observed structure of these coatings (Fig. 5) that suggest the presence of an hierarchical structure. ZnO is known to exhibit hydrophobic or hydrophilic behavior depending upon the structure it takes upon deposition (Myint et al., 2013). The low contact angle observed in the ZnO/PTFE samples suggest that ZnO exhibits a hydrophilic nature that lowers the observed contact angle as compared to PTFE. Additionally, ZnO/PTFE exhibited a more uniform structure and the lowest roughness among the samples. As a comparison, the Al substrate exhibited a contact angle of about 75°.

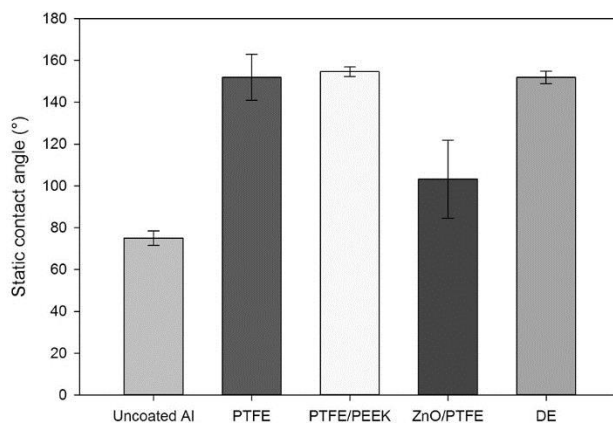


Figure 6. Wettability of coatings.

Friction and Wear Tests

Figure 7 shows the coefficient of friction exhibited by the samples against a tungsten probe. All coatings exhibited a significant decrease in friction response due to their lower surface-energy compared to aluminum. PTFE/PEEK exhibits a slightly higher value of friction response compared to PTFE, most likely due to the addition of PEEK

and due to the higher roughness of the sample, potentially adding a ratchetting contribution (Zhang et al., 2008b). ZnO/PTFE exhibits the lowest friction response, a result which differs from the findings by Li et al. (Li et al., 2001) which showed comparable response between PTFE and ZnO/PTFE composite films. The lowered roughness may contribute to a lesser ratchetting of ZnO/PTFE compared to PTFE leading to lower friction.

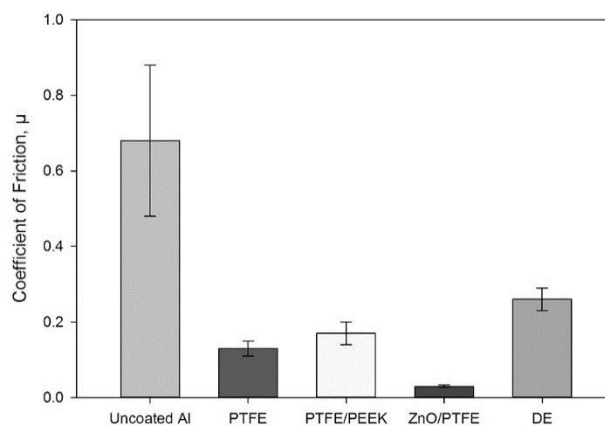


Figure 7. Frictional behavior of coatings.

Wear tests were conducted at a normal load of 40 mN for 10 and 25 cycles between a tungsten probe and the samples. Coatings were grinded mildly with 240-grit silicon carbide paper prior to wear tests in order to reduce the interference of high surface roughness during wear track depth measurements. Coating thickness measurements post-grinding showed that the amount of coating removed during grinding was negligible. The estimated average Hertzian contact pressure was 24 MPa, assuming a contact between tungsten and epoxy. Figure 8 shows the average wear track depth measured as a result of reciprocating wear tests for 10 and 25 cycles. The change in wear track depth after increasing the number of wear cycles for PTFE and

ZnO/PTFE was minimal which indicate good wear resistance for the given test conditions. DE and PTFE/PEEK coatings that exhibited higher roughness and friction properties, compared to PTFE and ZnO/PTFE coatings, were less resistant to wear and clearly showed an increase in wear track depth as the number of wear cycles were increased from 10 to 25 cycles.

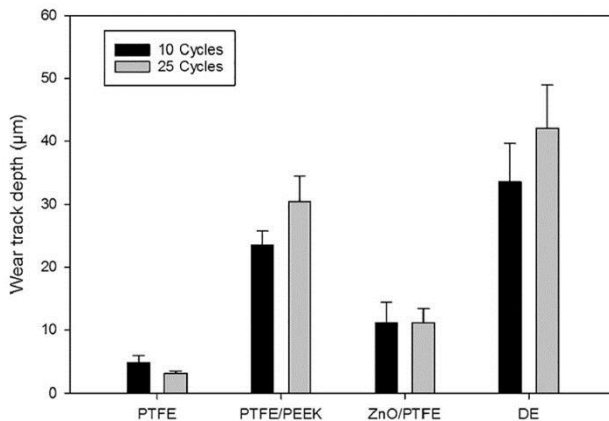


Figure 8. Wear track depth

Figure 9 shows the SEM micrographs of the wear track regions for the coated samples. The backscattered electron detector was configured to topo-mode to more clearly detect and image the wear track for all coatings except DE coatings to better view the wear tracks. There is a direct correlation between the wear track width and averaged wear track depth. As wear track depth increases, an increase in wear track width can be seen for the respective coatings in Figure 9. The SEM images for PTFE/PEEK, ZnO/PTFE, and DE coatings in Figure 9 show that asperities or particles within the wear area were removed as a result of the reciprocating wear. There was no evidence of material build-up along the sides of the wear track which would indicate ploughing, and EDS analysis of the probe tip did not detect chemical elements from the coatings which would indicate adhesive wear. The mode of wear for the wear tests can therefore be best classified as mildly abrasive. This abrasive phenomenon is less

apparent for the PTFE coating which exhibited the highest wear resistance of all the coatings.

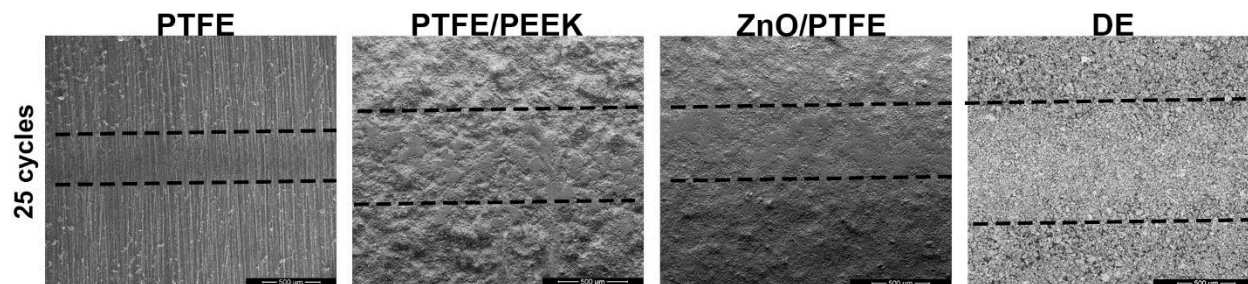


Figure 9. SEM micrographs of wear tracks on various samples for 25 cycles.

Conclusions

In this study, the wettability and tribological behavior of four candidate superhydrophobic coatings on Al substrates were investigated. All candidate coatings except ZnO/PTFE displayed superhydrophobic behavior with average static water contact angles higher than 150 degrees. The higher wettability of the ZnO/PTFE coating was attributed to the natural hydrophilic properties of an unstructured and continuous ZnO layer. Results suggest that the hierarchically-structured particles of the PTFE/PEEK and DE coatings resulted in measured R_a and friction values that were significantly higher than those of PTFE and ZnO/PTFE coatings that were composed of a single average particle size distribution and smaller particles, respectively.

The mutual consistency of wear track depth values and SEM images of the wear track areas suggest that PTFE and ZnO/PTFE coatings were more wear resistant than DE and PTFE/PEEK coatings. We hypothesize that the larger particles present in DE and PTFE/PEEK coatings may have resulted in weak interparticle bonding, thus leaving some particles unbound or loose on the surface. Further studies can expand upon the

effect of deposition parameters and coating compositions to provide further explanation for the physical attributes of superhydrophobic coatings that influence their mechanical wear resistance.

CHAPTER 4. DEVELOPMENT AND PERFORMANCE EVALUATION OF SUPERHYDROPHOBIC COATED CONCRETE

Synopsis, Scope, and Objective

The use of anti-icing and de-icing agents on PCC concrete roads has proven to be a fast and reliable means to controlling and preventing the adhesion of ice. However, the repeated use of sodium and calcium chlorides on concrete ultimately leads to corrosion and mechanical failure of the cementitious materials, and deicer runoff poses environmental threats to nearby water sources and wildlife (Kaushal et al., 2005, Ramakrishna and Viraraghavan, 2005, Panno et al., 2006, Fay and Shi, 2012, Kelly, 2008). High-traffic areas such as highways and airports that experience frequent snow and icing events during the winter season must employ and compensate hundreds of workers just for snow and ice removal. Such tasks also require snow removal equipment that costs millions of dollars and maintenance that requires additional funds and workers. The effects of deicers and road salt on concrete have been studied and reported upon extensively to properly address current challenges and begin to develop innovations that circumvent their use (Hassan et al., 2002, Shi et al., 2013). Calcium magnesium acetate (CMA) is a safer alternative road deicer to replace environmentally unacceptable NaCl and CaCl₂, but its high cost weakens its chance for widespread use (Dionysiou et al., 2000, Yang et al., 1992). Alternative technologies such as conductive concrete (Yehia and Tuan, 1999, Yehia et al., 2000, Yehia and Tuan, 2000, Yang et al., 2012), hydronic-heated pavements and the use of phase change materials for self-heated pavements are all viable options for minimizing the use of corrosive chemicals. Self-healing concretes that contain pre-incorporated healing agents, such as CaCO₃,

retard cracks caused by corrosive deicing chemicals. Such technologies carry expensive manufacturing and construction costs that are not viable for large-scale applications and require the demolition and removal of existing concrete which incur more expenses.

There is a need for a snow and ice removal process or technology that is durable, less invasive and requires less workforce, equipment, and maintenance. Recent studies have considered mimicking those surfaces found in nature that display extreme anti-wetting or superhydrophobic properties for mitigating ice adhesion on weather-exposed surfaces (Boinovich and Emelyanenko, 2013, Cao et al., 2009, Ferrick et al., 2008, Guo et al., 2012, Kulinich and Farzaneh, 2011, Saito et al., 1997). Several experimental procedures for fabricating superhydrophobic surfaces have been reported in the literature (Basu et al., 2011, Boinovich and Emelyanenko, 2013, Braziers.Pr et al., 1972, Chen et al., 2012, Crick and Parkin, 2011, Feng et al., 2003, Hatton and Aizenberg, 2012, Herminghaus, 2000, Hosono et al., 2005, Jin et al., 2005, Li et al., 2003, Pozzato et al., 2006, Saini et al., 2008, Saito et al., 1997, Shi et al., 2006, Shi et al., 2005, Shiu et al., 2004, Si and Xue, 2009, Somlo and Gupta, 2001, Srinivasan et al., 2008, Suh and Jon, 2005, Wang et al., 2007, Zhang et al., 2008a). The incorporation of superhydrophobic solutions within cementitious matrices has shown improved mechanical performance and improved durability characteristics in concrete due to the creation of an air void system with properties to resist several thousand freeze-thaw cycles, water absorption, and chloride permeability (Muzenski et al., 2015). However, this method is only applicable to the development of new concrete and requires the removal of existing ones. The use of coatings on concrete surfaces has the potential

advantages of being less invasive, low-maintenance, and more environmentally friendly. Studies report the development of concrete surfaces with high water repellency after depositing coatings consisting hydrophobic emulsions that exhibit a combination of hierarchical roughness and hydrophobicity (Flores-Vivian et al., 2013).

The first objective of this study was to establish base friction and roughness properties for PCC concrete using in-lab instruments. The next objective was to investigate possible changes in the roughness and frictional behavior of PCC concrete surfaces after being spray-coated with a superhydrophobic suspension. We also incorporated different dosages of a superhydrophobic admixture into a mortar mix design to evaluate possible changes in surface wettability and mechanical strength of the cured mortar specimens. The results from these experiments can be used to help guide future efforts in developing durable superhydrophobic concrete.

Research Methodology

Superhydrophobic Coatings for PCC Concrete Surfaces

PCC concrete specimens were mixed using a standard mix design which consisted of aggregate, cement, sand and water. A non-contact profilometer, which used white light interferometry to gather surface profile data, was used to measure the average surface roughness of the concrete samples. However, this method proved to be unsuccessful due to the profilometer's requirement for a substrate that is reflective. A thin layer of gold was deposited on concrete samples to increase reflectivity, but there were still many uncoated locations on the concrete surface that caused roughness measurements to be inefficient as seen in Figure 10. Additionally, the measured area of concrete was only 0.47 x 0.35 mm². Such a small area was not seen as representative of the entire concrete surface which is very heterogeneous.

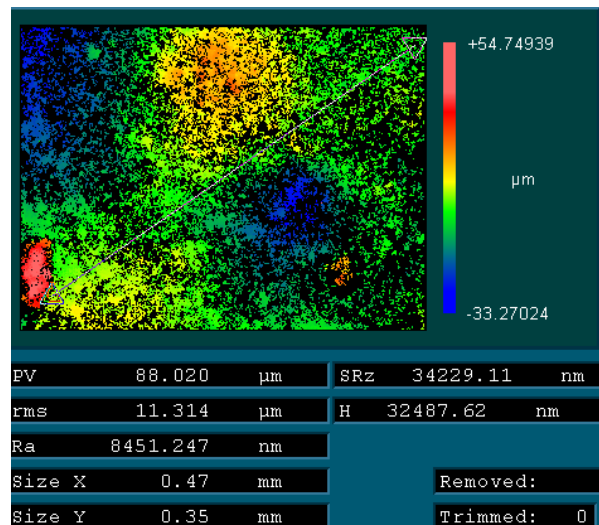


Figure 10. Surface map of concrete showing void areas.

It was determined that the natural roughness of the cured concrete specimens exceeded the measuring capabilities of the available contact and non-contact profilometers. However, uniform base roughness was required to avoid inaccurate measurements of frictional behavior in later tests. Therefore, the concrete surfaces were polished in order to achieve uniform surface roughness. A Buehler Ecomet III polisher/grinder was used to polish concrete specimens shown in Figure 11. Abrasive polishing pads with a grit size of 60 was used to polish the surface, and the speed (rpm) was constant for each polished sample. The loading force was manually applied by hand which led to some human error being present during the polishing process. A Dektak IIA contact profilometer was used to measure the average roughness on each of the samples to confirm whether or not a uniform roughness had been achieved after polishing the concrete surfaces. Table 4 shows that the variation among the measurements is lower than 30% for samples 1 and 3 but more than 40% for sample 2.



Figure 11. Polished concrete specimens

Table 3. Average roughness of polished concrete.

Average roughness of polished concrete surfaces	
Sample	Average Roughness, R_a (μm)
1	4.8 ± 1.2
2	4.9 ± 2.1
3	8.9 ± 2.4

The higher degree of variation in average roughness for sample 2 led us to believe that concrete polishing would not consistently yield polished surfaces with less than 30% variability of measured average roughness due to the human error that was present during the polishing process. A variation among average roughness measurements that is lower than 30% was desirable because this would provide proof that some other factor and not surface roughness was responsible for any significant changes in friction and roughness after coatings were applied to the substrate surface.

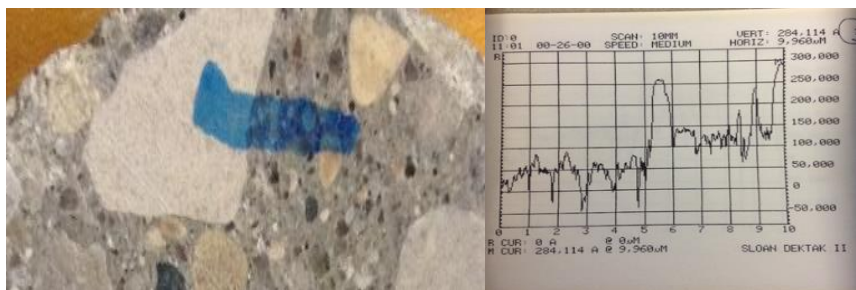


Figure 12. Left: Profilometer scan path from aggregate to cement/sand Right: Contact profilometer surface profile.

Figure 12 shows that the surface roughness increased by approximately 5 microns as the contact probe left the large aggregate and traveled over the rougher cement and

sand particles. It was concluded that unpolished and polished concrete was too rough for measurement using the in-lab profilometers in this frictional study.

In order to measure the frictional behavior of concrete, a larger concrete specimen which allowed for the use of a more traditional friction test was utilized. A suspension of PTFE and epoxy were spray-deposited on the concrete surface shown in Figure 13, and the British pendulum tester (BPM) was used to measure the resulting friction coefficient in wet and dry conditions after the coating dried.



Figure 12. Concrete slab for BPT testing.

The results in Figure 14 show that uncoated control concrete displays higher friction than the concrete coated with PTFE. The friction coefficient for both control and coated concrete was reduced after performing the BPT test in wet conditions. These results show that friction is reduced on concrete as a result of applying the superhydrophobic coating. Furthermore, the friction level on the concrete was reduced even more under wet conditions. Future experiments can extend the study to larger-scale concrete slabs where larger more accurate friction measuring tools can be implemented.

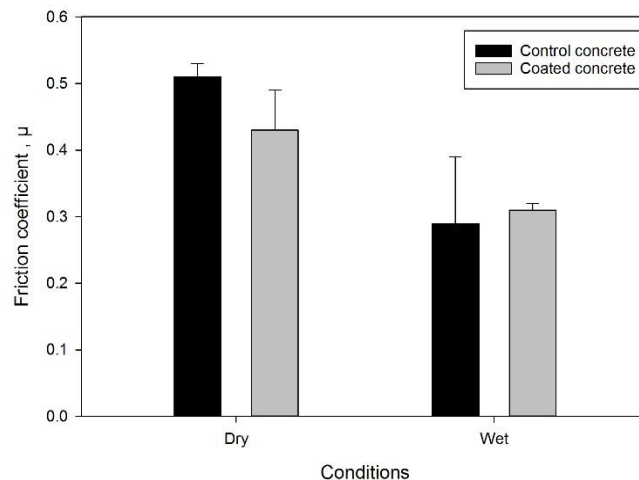


Figure 14. Friction coefficient of dry and wet coated concrete.

Although the high roughness of concrete did not allow for a lab-scale investigation, some concrete specimens were coated with the PTFE coating described in Chapter 3 in order to see the wettability of the coated concrete. Figure 15 shows that dyed water drops bead up on the coated portion of concrete and wet the uncoated portion.

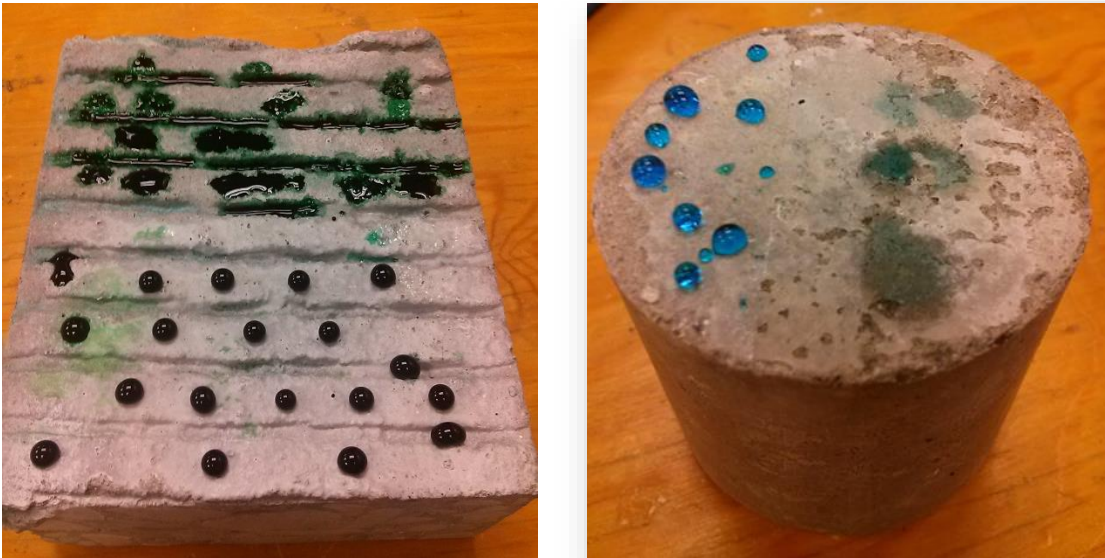


Figure 13. Left: Coating on textured concrete Right: Coating on untextured concrete.

Superhydrophobic Admixtures for Mortar Specimens

For this study, PTFE powder was incorporated into the mix design of mortar. Mortar consists of cement, sand, and water. Mortar samples containing 2 and 5% PTFE powder by weight of cement were mixed and cured. After 7-day curing, the PTFE-modified mortar samples were tested for compressive strength, surface friction, and surface roughness.

The results of the tests are shown in Table 5. The right image of Figure 16 shows that PTFE-induced mortar was less wettable than the control mortar sample. The 7-day compressive strengths of the 2 and 5% PTFE-induced mortar samples was 52 and 43 MPa, respectively. At 2% PTFE, the measured compressive strength for the mortar specimen was similar to that of the control mortar specimen. The decrease in compressive strength for the 5% PTFE-induced mortar specimen was attributed to a

higher dosage of PTFE which could have affected the hydration process of the mortar samples resulting in a lower 7-day compressive strength. An optical profilometer was used to measure the average surface roughness on both mortar samples. It was noticed that the four sides and bottom side of the cubed mortar samples had more reflective surfaces than the top surface. Therefore, one of the more reflective surfaces was used for gathering roughness data with the profilometer. Coincidentally, the measured average roughness of the 2 and 5% PTFE-induced mortar samples was 2 and 5 microns, respectively. It is hypothesized that the average roughness increased with the dosage of PTFE particles in the mortar mix. Next, a pin-on-flat micro tribometer was used to measure the average coefficient of friction on the two sample surfaces. A ramp load test was used to gather the data. The expectation was that the 5% PTFE-induced mortar sample would have a lower coefficient of friction than the 2% sample because the hydrophobic PTFE lower surface friction. A decrease in coefficient of friction was noticed for PTFE-induced mortar samples which was expected considering the low

surface energy of PTFE. However, there was little difference in friction between the 2 and 5% PTFE-induced mortar.

Table 4. Preliminary roughness, frictional, and strength study of PTFE-induced mortar.

Sample	Average Roughness (μm)	Coefficient of Friction	7-Day Strength (MPa)
Control	N/A	0.15 ± 0.01	50
2% PTFE	2	0.11 ± 0.01	52
5% PTFE	5	0.11 ± 0.01	43



Figure 14. Left: Mixing sand, cement, and water Right: Water on control and PTFE-treated mortar samples.

Conclusions

The heterogeneous nature of concrete did not allow for lab-scale friction and wear studies. However, we were able to gain some insight on the frictional behaviors of coated and uncoated concrete after applying coatings to a larger concrete slab and utilizing the British pendulum tester to measure the friction coefficient in wet and dry conditions. Results showed that the surface friction coefficient of concrete did decrease as a result of applying a PTFE coating, and the friction coefficient was further reduced when the measurements were made in wet conditions.

Mortar specimens containing 2 and 5% PTFE by weight of cement experienced an expected decrease in surface friction compared to a control sample. Although the PTFE-induced samples exhibited lower surface wettability, compressive strength tests showed that the compressive strength of the mortar samples decreased with higher dosages of PTFE.

CHAPTER 5. FUTURE RESEARCH AND RECOMMENDATIONS

Specific Findings and Limitations

All candidate coatings except ZnO/PTFE displayed superhydrophobic behavior with average static water contact angles higher than 150 degrees. The higher wettability of the ZnO/PTFE coating was attributed to the natural hydrophilic properties of an unstructured and continuous ZnO layer. Results suggest that the hierarchically-structured particles of the PTFE/PEEK and DE coatings resulted in measured R_a and friction values that were significantly higher than those of PTFE and ZnO/PTFE coatings that were composed of a single average particle size distribution and smaller particles, respectively.

The mutual consistency of wear track depth values and SEM images of the wear track areas suggest that PTFE and ZnO/PTFE coatings were more wear resistant than DE and PTFE/PEEK coatings. We hypothesize that the larger particles present in DE and PTFE/PEEK coatings may have resulted in weak interparticle bonding, thus leaving some particles unbound or loose on the surface. Further studies can expand upon the effect of deposition parameters and coating compositions to provide further explanation for the physical attributes of superhydrophobic coatings that influence their mechanical wear resistance.

The roughness of the natural surface of PCC concrete exceeded the capabilities of the contact profilometer and tribometer used in this study. Therefore concrete samples were polished to yield a smoother surface that could be measured with the

proposed instruments. However, it was found that the heterogeneous nature of concrete at the microscale presented challenges for measuring R_a and coefficient of friction values even when concrete was polished. This challenge prevented a small lab-scale study from being conducted, and a more traditional method of measuring the frictional behavior of concrete was carried out using the British pendulum tester. Results showed that the surface friction coefficient of concrete did decrease as a result of applying a PTFE coating, and the friction coefficient was further reduced when the measurements were made in wet conditions.

Preliminary studies of PTFE-induced mortar specimens gave valuable insight on the effect hydrophobic admixtures can have on the strength, friction and roughness properties, and wettability of cementitious materials. Mortar specimens containing 2 and 5% PTFE by weight of cement experienced an expected decrease in surface friction compared to a control sample. Although the PTFE-induced samples exhibited lower surface wettability, compressive strength tests showed that the compressive strength of the mortar samples decreased with higher dosages of PTFE.

Recommendations

Recommendations on Implementation for Airport Concrete Pavements

A detailed cost analysis for the implementation of large scale coatings will need to be conducted before superhydrophobic coatings are considered for use by airports or any other interested buyer. The cost analysis will have to account for cost of materials, maintenance, application equipment, and required personnel just to name a few. In order to get a rough idea of what these costs will entail, candidate coating systems will

need to be deployed at test sites and locations that host large-area test slabs. In this way engineers can begin to understand the associated challenges and generate estimates of the amount of material, equipment, and personnel that are required to produce and maintain this type of technology. This effort will require the continued collaborative efforts of both research engineers and airport managers. Our group has maintained good relations with local airports including Des Moines International Airport and Minneapolis St. Paul International Airport.

Role of Superhydrophobic Coatings in Hybrid Heated Airport Pavements

One major potential impact of superhydrophobic coatings for airport pavements is the possible reduction in costly destructive PCC concrete rehabilitations due to the pavement's exposure to high loads, annual freeze/thaw cycles, and de-icing/anti-icing salts. The potential reduction of ice/surface bonding by superhydrophobic coatings could also reduce the amount of power required of other heated pavement technologies to melt ice and snow away. Snow-removal equipment and airport personnel will be able to clear snow and ice from surfaces with greater ease thus reducing the number of weather-related flight delays and cancellations.

Other Potential Airport Applications

Superhydrophobic coatings should not only be limited to airport runways and taxiways. There are several other areas of airports that could benefit from this technology. Vertical surfaces such as solar panels, signs, windows, and aircrafts could also benefit. The durability of coatings on vertical surfaces would be less of an issue since exposure to large mechanical loads would be less. Other surfaces at airports like sidewalks and parking garages could also benefit from superhydrophobic coatings.

Such coatings would create a safer environment for travelers and potentially reduce ice-related slip-and-falls that may cost airports thousands of dollars each year.

Future Research Direction

Future studies could focus more on the development of icephobic coatings or finding relations between superhydrophobic and icephobic behavior of different coating materials. Once large-area test sites are identified, large-scale production and testing of superhydrophobic coatings can begin. Large-scale studies will have the benefit of providing more realistic behavior of coatings when they are exposed to large loads and extreme temperatures.

References

- BASU, M., SINHA, A. K., PRADHAN, M., SARKAR, S., NEGISHI, Y. & PAL, T. 2011. Fabrication and Functionalization of CuO for Tuning Superhydrophobic Thin Film and Cotton Wool. *Journal of Physical Chemistry C*, 115, 20953-20963.
- BOINOVICH, L. B. & EMELYANENKO, A. M. 2013. Anti-icing potential of superhydrophobic coatings. *Mendeleev Communications*, 23, 3-10.
- BRAZIER, P. R., LATHAM, J. & JENNINGS, S. G. 1972. Interaction of Falling Water Drops - Coalescence. *Proceedings of the Royal Society of London Series A - Mathematical and Physical Sciences*, 326, 393-&.
- CAO, L. L., JONES, A. K., SIKKA, V. K., WU, J. Z. & GAO, D. 2009. Anti-Icing Superhydrophobic Coatings. *Langmuir*, 25, 12444-12448.
- CASSIE, A. B. D. & BAXTER, S. 1944. Wettability of porous surfaces. *Transactions of the Faraday Society*, 40, 0546-0550.
- CHEN, L. S., WANG, C. J. & CHEN, G. R. 2012. Controlled growth of carbon spheres by chemical vapor deposition based on anodic aluminum oxide nano-template. *Frontiers of Mechanical Engineering and Materials Engineering, Pts 1 and 2*, 184-185, 924-927.
- CRICK, C. R. & PARKIN, I. P. 2011. CVD of copper and copper oxide thin films via the in situ reduction of copper (II) nitrate-a route to conformal superhydrophobic coatings. *Journal of Materials Chemistry*, 21, 14712-14716.

- DAI, S. X., ZHANG, D. B., SHI, Q., HAN, X., WANG, S. J. & DU, Z. L. 2013. Biomimetic fabrication and tunable wetting properties of three-dimensional hierarchical ZnO structures by combining soft lithography templated with lotus leaf and hydrothermal treatments. *Crystengcomm*, 15, 5417-5424.
- DIONYSIOU, D. D., TSIANOU, M. & BOTSARIS, G. D. 2000. Investigation of the conditions for the production of calcium magnesium acetate (CMA) road deicer in an extractive crystallization process. *Crystal Research and Technology*, 35, 1035-1049.
- DU, L. X. & FOLLIARD, K. J. 2005. Mechanisms of air entrainment in concrete. *Cement and Concrete Research*, 35, 1463-1471.
- FANG, W. J., MAYAMA, H. & TSUJII, K. 2007. Spontaneous formation of fractal structures on triglyceride surfaces with reference to their super water-repellent properties. *Journal of Physical Chemistry B*, 111, 564-571.
- FAY, L. & SHI, X. M. 2012. Environmental Impacts of Chemicals for Snow and Ice Control: State of the Knowledge. *Water Air and Soil Pollution*, 223, 2751-2770.
- FENG, L., SONG, Y. L., ZHAI, J., LIU, B. Q., XU, J., JIANG, L. & ZHU, D. B. 2003. Creation of a superhydrophobic surface from an amphiphilic polymer. *Angewandte Chemie-International Edition*, 42, 800-802.
- FERRICK, M. G., MULHERIN, N. D., HAEHNEL, R. B., COUTERMARSH, B. A., DURELL, G. D., TANTILLO, T. J., CURTIS, L. A., CLAIR, T. L. S., WEISER, E. S., CANO, R. J., SMITH, T. M. & MARTINEZ, E. C. 2008. Evaluation of ice release coatings at cryogenic temperature for the space shuttle. *Cold Regions Science and Technology*, 52, 224-243.
- FLORES-VIVIAN, I., HEJAZI, V., KOZHUKHOVA, M. I., NOSONOVSKY, M. & SOBOLEV, K. 2013. Self-Assembling Particle-Siloxane Coatings for Superhydrophobic Concrete. *Acs Applied Materials & Interfaces*, 5, 13284-13294.
- GEMICI, Z., SHIMOMURA, H., COHEN, R. E. & RUBNER, M. F. 2008. Hydrothermal treatment of nanoparticle thin films for enhanced mechanical durability. *Langmuir*, 24, 2168-2177.
- GUO, P., ZHENG, Y. M., WEN, M. X., SONG, C., LIN, Y. C. & JIANG, L. 2012. Icephobic/Anti-Icing Properties of Micro/Nanostructured Surfaces. *Advanced Materials*, 24, 2642-2648.
- HASSAN, Y., EL HALIM, A. O. A., RAZAQPUR, A. G., BEKHEET, W. & FARHA, M. H. 2002. Effects of runway deicers on pavement materials and mixes: Comparison with road salt. *Journal of Transportation Engineering-Asce*, 128, 385-391.
- HATTON, B. D. & AIZENBERG, J. 2012. Writing on Superhydrophobic Nanopost Arrays: Topographic Design for Bottom-up Assembly. *Nano Letters*, 12, 4551-4557.
- HEJAZI, V., SOBOLEV, K. & NOSONOVSKY, M. 2013. From superhydrophobicity to icephobicity: forces and interaction analysis. *Scientific Reports*, 3.

- HERMINGHAUS, S. 2000. Roughness-induced non-wetting. *Europhysics Letters*, 52, 165-170.
- HORGNIES, M. & CHEN, J. J. 2014. Superhydrophobic concrete surfaces with integrated microtexture. *Cement & Concrete Composites*, 52, 81-90.
- HOSONO, E., FUJIHARA, S., HONMA, I. & ZHOU, H. S. 2005. Superhydrophobic perpendicular nanopin film by the bottom-up process. *Journal of the American Chemical Society*, 127, 13458-13459.
- JIANG, D. Y., TIAN, C. G., LIU, Q. F., ZHAO, M., QIN, J. M., HOU, J. H., GAO, S., LIANG, Q. C. & ZHAO, J. X. 2014. Young's modulus of individual ZnO nanowires. *Materials Science and Engineering a-Structural Materials Properties Microstructure and Processing*, 610, 1-4.
- JIN, M. H., FENG, X. J., FENG, L., SUN, T. L., ZHAI, J., LI, T. J. & JIANG, L. 2005. Superhydrophobic aligned polystyrene nanotube films with high adhesive force. *Advanced Materials*, 17, 1977-+.
- JUNG, S., DORRESTIJN, M., RAPS, D., DAS, A., MEGARIDIS, C. M. & POULIKAKOS, D. 2011. Are Superhydrophobic Surfaces Best for Icephobicity? *Langmuir*, 27, 3059-3066.
- JUNG, S., TIWARI, M. K., DOAN, N. V. & POULIKAKOS, D. 2012. Mechanism of supercooled droplet freezing on surfaces. *Nature Communications*, 3.
- JUNG, Y. C. & BHUSHAN, B. 2009. Mechanically Durable Carbon Nanotube-Composite Hierarchical Structures with Superhydrophobicity, Self-Cleaning, and Low-Drag. *Acs Nano*, 3, 4155-4163.
- KAUSHAL, S. S., GROFFMAN, P. M., LIKENS, G. E., BELT, K. T., STACK, W. P., KELLY, V. R., BAND, L. E. & FISHER, G. T. 2005. Increased salinization of fresh water in the northeastern United States. *Proceedings of the National Academy of Sciences of the United States of America*, 102, 13517-13520.
- KELLY, W. R. 2008. Long-term trends in chloride concentrations in shallow aquifers near Chicago. *Ground Water*, 46, 772-781.
- KULINICH, S. A. & FARZANEH, M. 2011. On ice-releasing properties of rough hydrophobic coatings. *Cold Regions Science and Technology*, 65, 60-64.
- LAZNIEWSKA-PIEKARCZYK, B. 2012. The influence of selected new generation admixtures on the workability, air-voids parameters and frost-resistance of self compacting concrete. *Construction and Building Materials*, 31, 310-319.
- LI, F., HU, K. A., LI, J. L. & ZHAO, B. Y. 2001. The friction and wear characteristics of nanometer ZnO filled polytetrafluoroethylene. *Wear*, 249, 877-882.
- LI, M., ZHAI, J., LIU, H., SONG, Y. L., JIANG, L. & ZHU, D. B. 2003. Electrochemical deposition of conductive superhydrophobic zinc oxide thin films. *Journal of Physical Chemistry B*, 107, 9954-9957.
- MAKKONEN, L. 2013. A model of hoarfrost formation on a cable. *Cold Regions Science and Technology*, 85, 256-260.
- MANCA, M., CANNAVALE, A., DE MARCO, L., ARICO, A. S., CINGOLANI, R. & GIGLI, G. 2009. Durable Superhydrophobic and Antireflective Surfaces by

- Trimethylsilanized Silica Nanoparticles-Based Sol-Gel Processing. *Langmuir*, 25, 6357-6362.
- MENINI, R. & FARZANEH, M. 2009. Elaboration of Al₂O₃/PTFE icephobic coatings for protecting aluminum surfaces. *Surface & Coatings Technology*, 203, 1941-1946.
- MEULER, A. J., SMITH, J. D., VARANASI, K. K., MABRY, J. M., MCKINLEY, G. H. & COHEN, R. E. 2010. Relationships between Water Wettability and Ice Adhesion. *Acs Applied Materials & Interfaces*, 2, 3100-3110.
- MUZENSKI, S., FLORES-VIVIAN, I. & SOBOLEV, K. 2015. Durability of superhydrophobic engineered cementitious composites. *Construction and Building Materials*, 81, 291-297.
- MYINT, M. T. Z., KUMAR, N. S., HORNYAK, G. L. & DUTTA, J. 2013. Hydrophobic/hydrophilic switching on zinc oxide micro-textured surface. *Applied Surface Science*, 264, 344-348.
- OLIVEIRA, N. M., REIS, R. L. & MANO, J. F. 2013. Superhydrophobic Surfaces Engineered Using Diatomaceous Earth. *Acs Applied Materials & Interfaces*, 5, 4202-4208.
- PANNO, S. V., HACKLEY, K. C., HWANG, H. H., GREENBERG, S. E., KRAPAC, I. G., LANDSBERGER, S. & O'KELLY, D. J. 2006. Source identification of sodium and chloride in natural waters: Preliminary results. *Ground Water*, 44, 176-187.
- PILIPAVICIUS, J., KAZADOJEV, I., BEGANSKIENE, A., MELNINKAITIS, A., SIRUTKAITIS, V. & KAREIVA, A. 2008. Hydrophobic Antireflective Silica Coatings via Sol-gel Process. *Materials Science-Medziagotyra*, 14, 283-287.
- POLIZOS, G., WINTER, K., LANCE, M. J., MEYER, H. M., ARMSTRONG, B. L., SCHAEFFER, D. A., SIMPSON, J. T., HUNTER, S. R. & DATSKOS, P. G. 2014. Scalable superhydrophobic coatings based on fluorinated diatomaceous earth: Abrasion resistance versus particle geometry. *Applied Surface Science*, 292, 563-569.
- POZZATO, A., DAL ZILIO, S., FOIS, G., VENDRAMIN, D., MISTURA, G., BELOTTI, M., CHEN, Y. & NATALI, M. 2006. Superhydrophobic surfaces fabricated by nanoimprint lithography. *Microelectronic Engineering*, 83, 884-888.
- RAMAKRISHNA, D. M. & VIRARAGHAVAN, T. 2005. Environmental impact of chemical deicers - A review. *Water Air and Soil Pollution*, 166, 49-63.
- SAINI, G., SAUTTER, K., HILD, F. E., PAULEY, J. & LINFORD, M. R. 2008. Two-silane chemical vapor deposition treatment of polymer, (nylon) and oxide surfaces that yields hydrophobic, (and superhydrophobic), abrasion-resistant thin films. *Journal of Vacuum Science & Technology A*, 26, 1224-1234.
- SAITO, H., TAKAI, K. & YAMAUCHI, G. 1997. Water- and ice-repellent coatings. *Surface Coatings International*, 80, 168-+.
- SAN VICENTE, G., BAYON, R., GERMAN, N. & MORALES, A. 2009. Long-term durability of sol-gel porous coatings for solar glass covers. *Thin Solid Films*, 517, 3157-3160.

- SHI, F., SONG, Y. Y., NIU, J., XIA, X. H., WANG, Z. Q. & ZHANG, X. 2006. Facile method to fabricate a large-scale superhydrophobic surface by galvanic cell reaction. *Chemistry of Materials*, 18, 1365-1368.
- SHI, F., WANG, Z. Q. & ZHANG, X. 2005. Combining a layer-by-layer assembling technique with electrochemical deposition of gold aggregates to mimic the legs of water striders. *Advanced Materials*, 17, 1005-+.
- SHI, X. M., VENEZIANO, D., XIE, N. & GONG, J. 2013. Use of chloride-based ice control products for sustainable winter maintenance: A balanced perspective. *Cold Regions Science and Technology*, 86, 104-112.
- SHIBUICHI, S., ONDA, T., SATOH, N. & TSUJII, K. 1996. Super water-repellent surfaces resulting from fractal structure. *Journal of Physical Chemistry*, 100, 19512-19517.
- SHIU, J. Y., KUO, C. W., CHEN, P. L. & MOU, C. Y. 2004. Fabrication of tunable superhydrophobic surfaces by nanosphere lithography. *Chemistry of Materials*, 16, 561-564.
- SI, Y. F. & XUE, D. F. 2009. HYDROTHERMAL FABRICATION OF CORE-SHELL STRUCTURED Cu_2O MICROSPHERES VIA AN INTERMEDIATE-TEMPLATE ROUTE. *Modern Physics Letters B*, 23, 3851-3858.
- SOMLO, B. & GUPTA, V. 2001. A hydrophobic self-assembled monolayer with improved adhesion to aluminum for deicing application. *Mechanics of Materials*, 33, 471-480.
- SONG, H. J., ZHANG, Z. Z. & MEN, X. H. 2008. Superhydrophobic PEEK/PTFE composite coating. *Applied Physics a-Materials Science & Processing*, 91, 73-76.
- SRINIVASAN, S., PRAVEEN, V. K., PHILIP, R. & AJAYAGHOSH, A. 2008. Bioinspired superhydrophobic coatings of carbon nanotubes and linear pi systems based on the "bottom-up" self-assembly approach. *Angewandte Chemie-International Edition*, 47, 5750-5754.
- SUH, K. Y. & JON, S. 2005. Control over wettability of polyethylene glycol surfaces using capillary lithography. *Langmuir*, 21, 6836-6841.
- VAN DEN HEEDE, P., FURNIERE, J. & DE BELIE, N. 2013. Influence of air entraining agents on deicing salt scaling resistance and transport properties of high-volume fly ash concrete. *Cement & Concrete Composites*, 37, 293-303.
- WANG, D. A., GUO, Z. G., CHEN, Y. M., HAO, J. & LIU, W. M. 2007. In situ hydrothermal synthesis of nanolamellate CaTiO_3 with controllable structures and wettability. *Inorganic Chemistry*, 46, 7707-7709.
- WENZEL, R. N. 1936. Resistance of solid surfaces to wetting by water. *Industrial and Engineering Chemistry*, 28, 988-994.
- WU, Y. Y., BEKKE, M., INOUE, Y., SUGIMURA, H., KITAGUCHI, H., LIU, C. S. & TAKAI, O. 2004. Mechanical durability of ultra-water-repellent thin film by microwave plasma-enhanced CVD. *Thin Solid Films*, 457, 122-127.
- XIU, Y. H., LIU, Y., BALU, B., HESS, D. W. & WONG, C. P. 2012. Robust Superhydrophobic Surfaces Prepared with Epoxy Resin and Silica

- Nanoparticles. *Ieee Transactions on Components Packaging and Manufacturing Technology*, 2, 395-401.
- YANG, S. T., ZHU, H., LEWIS, V. P. & TANG, I. C. 1992. Calcium Magnesium Acetate (Cma) Production from Whey Permeate - Process and Economic-Analysis. *Resources Conservation and Recycling*, 7, 181-200.
- YANG, T., YANG, Z. J., SINGLA, M., SONG, G. B. & LI, Q. 2012. Experimental Study on Carbon Fiber Tape-Based Deicing Technology. *Journal of Cold Regions Engineering*, 26, 55-70.
- YEHIA, S. & TUAN, C. Y. 1999. Conductive concrete overlay for bridge deck deicing. *Aci Materials Journal*, 96, 382-390.
- YEHIA, S., TUAN, C. Y., FERDON, D. & CHEN, D. 2000. Conductive concrete overlay for bridge deck deicing: Mixture proportioning, optimization, and properties. *Aci Materials Journal*, 97, 172-181.
- YEHIA, S. A. & TUAN, C. Y. 2000. Thin conductive concrete overlay for bridge deck deicing and anti-icing. *Concrete 2000*, 45-53.
- ZHANG, D. S. 1996. Air entrainment in fresh concrete with PFA. *Cement & Concrete Composites*, 18, 409-416.
- ZHANG, X., SHI, F., NIU, J., JIANG, Y. G. & WANG, Z. Q. 2008a. Superhydrophobic surfaces: from structural control to functional application. *Journal of Materials Chemistry*, 18, 621-633.
- ZHANG, Z., CHEN, X. & WANG, T. 2008b. A simple constitutive model for cyclic compressive ratchetting deformation of polytetrafluoroethylene (PTFE) with stress rate effects. *Polymer Engineering and Science*, 48, 29-36.
- ZHENG, L. Q., LI, Z. R., BOURDO, S., KHEDIR, K. R., ASAR, M. P., RYERSON, C. C. & BIRIS, A. S. 2011. Exceptional Superhydrophobicity and Low Velocity Impact Icephobicity of Acetone-Functionalized Carbon Nanotube Films. *Langmuir*, 27, 9936-9943.